

A facile synthesis of heteroatom-doped carbon framework anchored with TiO₂ nanoparticles for high performance lithium ion battery anodes

Bo Long · Song Chen · Biao Wang · Jingjing Tang · Juan Yang · Xiangyang Zhou

Received: 1 February 2018 / Accepted: 30 May 2018 / Published online: 14 June 2018
© Springer Science+Business Media B.V., part of Springer Nature 2018

Abstract Titanium dioxide (TiO₂)-based materials have been well studied because of the high safety and excellent cycling performance when employed as anode materials for lithium ion batteries (LIBs), whereas, the relatively low theoretical capacity (only 335 mAh g⁻¹) and serious kinetic problems such as poor electrical conductivity ($\sim 10^{-13}$ S cm⁻¹) and low lithium diffusion coefficient ($\sim 10^{-9}$ to 10^{-13} cm² s⁻¹) hinder the development of the TiO₂-based anode materials. To overcome these drawbacks, we present a facile strategy to synthesize N/S dual-doping carbon framework anchored with TiO₂ nanoparticles (NSC@TiO₂) as LIBs anode. Typically, TiO₂ nanoparticles are anchored into the porous graphene-based sheets with N, S dual doping feature, which is produced by carbonization and KOH activation process. The as-obtained NSC@TiO₂ electrode exhibits a high specific capacity of 250 mAh g⁻¹ with a coulombic efficiency of 99% after 500 cycles at 200 mA g⁻¹ and excellent rate performance, indicating its promising as anode material for LIBs.

Keywords Lithium ion batteries · N/S dual-doping · Nanoparticles · Anode materials · Energy storage

Introduction

Rechargeable lithium ion batteries (LIBs) are considerably interest owing to their relatively high energy density and environmental friendliness, compared with other energy storage devices for electric vehicles (EVs) (Tarascon and Armand 2001; Aricò et al. 2005; Larcher and Tarascon 2015). However, the current commercialized graphite anode with a low operating voltage versus Li/Li⁺, which results in the generation of lithium dendrite during the overcharge process, leading to serious safety problem (Zhou et al. 2016). Another safety problem comes from the thermal instability of solid electrolyte interphase (SEI) film generated on the surface of graphite at 0.8 V (Chen et al. 2013), which approaches to disintegrate at a low temperature (around 60 °C) and directly expose lithiated graphite to the non-aqueous electrolyte, causing a persistent thermopositive reaction (Wu et al. 2016). Thus, it cannot meet the demand for electronic devices with different functionalities such as hybrid electric vehicles, wearable electronics and other system (Yang et al. 2016). Taking this into consideration, titanium dioxide (TiO₂) has drawn particular interest owing to its high operating voltage (1.78 V vs. Li⁺/Li), which can prevent the generation of the SEI layer and lithium deposition on the anode (Armand and Tarascon 2008; Belharouak et al. 2007). Besides, TiO₂ is a zero-strain insertion material which means admirable reversibility, high safety, and stability during electrochemical processes. However, the development of a practical TiO₂ material for commercialization is still limited due to its low theoretical capacity

B. Long · S. Chen · B. Wang · J. Tang · J. Yang · X. Zhou (✉)
School of Metallurgy and Environment, Central South University, Changsha 410083, China
e-mail: hncsjy308@163.com

(336 mAh g⁻¹), poor electrical conductivity (~ 10⁻¹³ S cm⁻¹), and low lithium diffusion coefficient (~ 10⁻⁹ to 10⁻¹³ cm² s⁻¹) (Wagemaker et al. 2009; Kamata et al. 1999).

Over the years, extensive strategies have been devoted to handle the above problems. It is well known that interfacial design and the nanoscale regime interface can tune the electronic transport properties (Jannik and Maier 2004; Beaulieu et al. 2000); TiO₂ has been engineered into nanostructured materials such as nanowires, nanosheet, and nanorods. Compared with bulk materials, nanoscaled TiO₂ has a unique quantum size effect and surface effect, which can greatly increase the specific surface area for shortening the ion diffusion pathway (Shen et al. 2011; Zhao et al. 2011; Mi et al. 2011; Jung et al. 2011). However, due to the large surface free energy of nanoparticles, severe aggregation may take place during the charge-discharge process, weakening the favorable features of nanoscaled TiO₂ anodes. Therefore, it is still a great challenge to utilize TiO₂ nanostructures as anode in LIBs to settle the aggregation problem and the intrinsic low electronic conductivity (Chu et al. 2016). Due to the high conductivity of carbonaceous materials, substantial efforts have been made to construct various TiO₂/C nanostructures, in which carbon serves as framework to promote the electron transport ability and the aggregation of TiO₂ nanostructures is well addressed. For instance, Qiu and co-workers reported on TiO₂ nanocrystals grown in situ on a graphene aerogel surface, the strong interaction between TiO₂ and graphene aerogel and the improved electrical conductivity results in a good capacity of 204 mAh g⁻¹ at constant current densities of 0.1 Ag⁻¹ (Qiu et al. 2014).

Although improved electrochemical properties of TiO₂/C nanocomposites have been demonstrated, the conductivity of carbon matrix is still insufficient because of the low pyrolysis temperature, which greatly influences the reactivity and electric transfer ability and hence, the lithium storage capacity. Doping carbon with other heteroatoms (N, S, P, and B) has been supposed to be a potential material for energy storage devices (Wang et al. 2014a, b, 2015a, b; Yu et al. 2015; Yun et al. 2014). Nitrogen-doping of carbon has been extensively studied that exhibits excellent performance due to the better electronic conductivity. However, nitrogen-doped carbon materials still face a bottleneck of low capacity (Ma et al. 2014). Dual-doped carbon can dramatically improve the electrical conductivity performance and the

lithium storage performance due to the higher electronegativity and the structural defects (Wang et al. 2014a, b; Xing et al. 2015; Zhuang et al. 2015). Therefore, the rational design of TiO₂/C nanocomposites and the incorporation of heteroatoms in carbon matrix are both of great significance for obtaining high electrochemical property as anode in LIBs.

In this work, nano-TiO₂ anchored on N/S dual-doped carbon framework (NSC@TiO₂) was achieved via a facile method as high performance anode material for LIBs. N/S dual-doped carbon framework (NSC) was prepared by the carbonization of sucrose on graphene sheets with the addition of thiourea as N and S sources subsequent with KOH activation process. In situ hydrolysis of tetrabutyl titanate followed by calcination realized the anchoring of nano-TiO₂ on the surface of NSC. The homogeneous immobilization of nano-TiO₂ on NSC can enhance electronic conductivity and prevent the aggregation of graphene and TiO₂ nanoparticles over repeated discharge/charge processes. The anchored nano-TiO₂ with a diameter of 6–8 nm can facilitate the electron and ion transfer hence improves the electrochemical reactivity. Benefiting from the unique nanostructure, the NSC@TiO₂ composite exhibits a high reversible capacity of 250 mAh g⁻¹ at 1 C after 500 cycles, and good rate capacity up to 142 mAh g⁻¹ at 5 C when evaluated as anode or LIBs.

Experimental section

All the chemicals in this work were analytical reagents without further purification. All the solutions were prepared with deionized water.

Synthesis of GO

GO was synthesized according to the modified Hummers method (Hummers Jr and Offeman 1958). Briefly, 1 g of graphite powders, 1 g of NaNO₃, and 40 ml of concentrated H₂SO₄ were well mixed. After vigorous stirring at 0 °C for 1 h, 4 g of KMnO₄ was added gradually and the solution was left under stirring for 0.5 h. Then the mixture was transferred to 35 °C with stirring for 3 h. After that, 80 ml of deionized water was added, the temperature was up to 90 °C and maintained for 15 min. Then 5 ml of H₂O₂ was added, the product was centrifuged and washed by deionized water to obtain GO.

Synthesis of N- and S-doped carbons (NSC)

Typically, thiourea ($\text{CN}_2\text{H}_4\text{S}$) was used as precursor to synthesize N, S co-doped carbon through a hydrothermal process. The graphene oxide suspension was obtained by ultrasonic of the obtained GO with deionized water for 1 h. 4.8 g of sucrose and 350 mg of thiourea were dissolved into 70 ml of GO suspension (3 mg ml^{-1}), then sonicated for 1 h to get uniformly dispersed. Under vigorous stirring at room temperature for 4 h, the suspension was transferred into a Teflon-lined stainless steel autoclave (100 ml) and subsequently heated in a vacuum oven at $180 \text{ }^\circ\text{C}$ for 12 h under the static station. After being cooled down to the room temperature, the product was washed and filtered with DI water thoroughly and then dried at $60 \text{ }^\circ\text{C}$ for 12 h. The intermediate product and KOH with a ratio of 1:5 were mixed together and calcined at $800 \text{ }^\circ\text{C}$ for 1 h under argon atmosphere. The obtained dark powder was collected by washed to neutral and dried overnight.

Synthesis of the pure TiO_2

Typically, 3 ml of TBOT (tetrabutyl titanate) was added drop by drop into 10 ml of ethanol with vigorous stirring at $80 \text{ }^\circ\text{C}$ for 24 h in a water bath. The as-prepared powder was then heated at $500 \text{ }^\circ\text{C}$ with a heating rate of $5 \text{ }^\circ\text{C min}^{-1}$ in Ar atmosphere to obtain pure TiO_2 .

Synthesis of NSC@ TiO_2

Briefly, 0.2 g of the as-prepared NSC material was added into 500 ml of ethanol and sonicated for 1 h, then 4 ml of TBOT was added dropwise to hydrolyze to yield the precursor of TiO_2 , 1 ml of glacial acetic acid was used to adjust the pH and control the hydrolysis to get homogenous product. Under vigorous stirring for 24 h at $60 \text{ }^\circ\text{C}$, the mixture was washed with deionized water for three times, the obtained product was dried in an oven at $60 \text{ }^\circ\text{C}$ for 12 h. The powder was calcined at $500 \text{ }^\circ\text{C}$ for 1 h in Ar atmosphere to form the anatase titania, the sample was denoted as NSC@ TiO_2 .

Characterization

The SDTQ600 analyzer was applied to obtain thermogravimetric analysis (TGA) data in air at a heating rate

of $5 \text{ }^\circ\text{C min}^{-1}$ from room temperature to $800 \text{ }^\circ\text{C}$. The crystalline phase was characterized by X-ray diffraction (XRD, Rigaku-TTRIII) with Cu $K\alpha$ radiation ranging from 20° to 85° . The Raman tests were recorded with a LabRAM Hr800 (HORIBA JOBIN YVON, Korea). Nitrogen adsorption–desorption isotherms were performed using Quantachrome Nova Win 2 equipment to measure the surface area. The morphologies and structures were conducted using scanning electron microscope (SEM, JSM-6360), transmission electron microscope (TEM, JEM-2100F) and high resolution transmission electron microscope (HRTEM, Titan G2 60-300, Holland). X-ray photoelectron spectroscopy (XPS) measurements were carried out on an X-ray photoelectron spectrometer (K-Alpha 1063) with Al $K\alpha$ radiation to reveal the surface chemical species. The nitrogen adsorption and desorption isotherms were performed by using Quantachrome Nova Win 2 equipment.

Electrochemical measurement

The lithium storage experiments were carried out utilizing CR2025 coin-type cells. For the preparation of the working electrodes, active material (NSC, TiO_2 , or NSC@ TiO_2), acetylene black and polyvinylidene fluoride (PVDF) in a mass ratio of 8:1:1 mixed in N-methyl-2-pyrrolidinone to obtain the slurry. The slurry was subsequently spread uniformly on a Cu foil and then dried at $60 \text{ }^\circ\text{C}$ for 12 h. The mass loading of active material is about $1.0\text{--}1.2 \text{ mg cm}^{-2}$ in the working electrodes. 1 M LiPF_6 in ethylene carbonate (EC)/diethyl carbonate (DEC)/dimethyl carbonate (DMC) with a volume ratio of 1:1:1 was used as electrolyte. Li foil was working as both the counter electrode and the reference electrode; the coin cells were assembled in a glove box filled with argon atmosphere. Cyclic voltammograms (CV) were conducted in the potential range from 0.01 to 3 V (Vs Li/Li^+) at a scan rate of 0.2 mV s^{-1} on an electrochemical workstation (CHI660E). The electrode performance was carried out within a voltage range of 0.01–3.0 V (vs. Li/Li^+) by the galvanostatic method using the LAND CCT-2001A battery test system. Electrochemical impedance spectral (EIS) data was performed by an electrochemical workstation Princeton Applied Research Versa MC 2000 at a frequency range from 100 kHz to 10 mHz.

Results and discussion

The morphologies of the as-prepared NSC and NSC@TiO₂ samples were confirmed with SEM and TEM. As shown in Fig. 1a, b, as-prepared NSC displayed a typical two-dimensional wrinkled sheet with a lateral size up to 3 μm. The smooth surface of NSC demonstrated the homogeneous coating of thin carbon layer derived from sucrose on graphene sheets. After the anchoring of TiO₂ nanoparticles, the obtained NSC@TiO₂ composite exhibited the similar free-standing sheet-like structure (Fig. 1c). From the TEM images (Fig. 1d, e), it is apparent that TiO₂ nanoparticles with a diameter of 6–8 nm are decorated on the surface of NSC, of which the size of TiO₂ nanoparticles are much smaller than of the pure anatase TiO₂ synthesized from hydrolysis (Fig. 1). The lattice fringes with a spacing of 0.355 nm is well-matched with the (101) plane of anatase TiO₂ (Fig. 1e), whereas no significant crystalline plane of carbon is found, suggesting its amorphous nature. The selected area electron diffraction (SAED) patterns were employed to confirm the presence of graphene and TiO₂ species. The corresponding SEM elemental mapping images of the NSC@TiO₂ are shown in Fig. 1f to further examine the existence of Ti, C, S, N, and O, indicating the homogeneous distribution of these elements in the NSC@TiO₂.

The XRD patterns are showed in Fig. 2a to present the crystallographic structure of the as-prepared TiO₂ from the hydrolysis and the sample NSC@TiO₂. The well-defined peaks located at 25.3°, 36.9°, 37.7°, 38.5°, 48.0°, 53.8°, 55.0°, 62.1°, 62.6°, 68.7°, 70.2°, 74.0°, and 75.0° are indexed to the (101), (103), (004), (112), (200), (105), (211), (213), (204), (116), (220), (107), and (215) lattice planes of the anatase phase, TiO₂ [amd (141) space group, JCPDS#65-5714]. The strong peak at 25.3° can be ascribed to the regular space arrangement of the anatase TiO₂. The constant peak position for the NSC@TiO₂ indicates that the phase structure of TiO₂ has not been changed. A little peak at about 30.9° in the patterns of the NSC@TiO₂ could be assigned to the introduction of N/S functional groups. No significant peaks of carbon are observed even after the precursor was heated under Ar atmosphere. This result is consistent with the HRTEM observation. Thermo gravimetric analysis (TGA) was conducted to examine the carbon content in the NSC@TiO₂. As is shown in Fig. 2, the moisture in the sample was removed when the temperature was below 150 °C, the

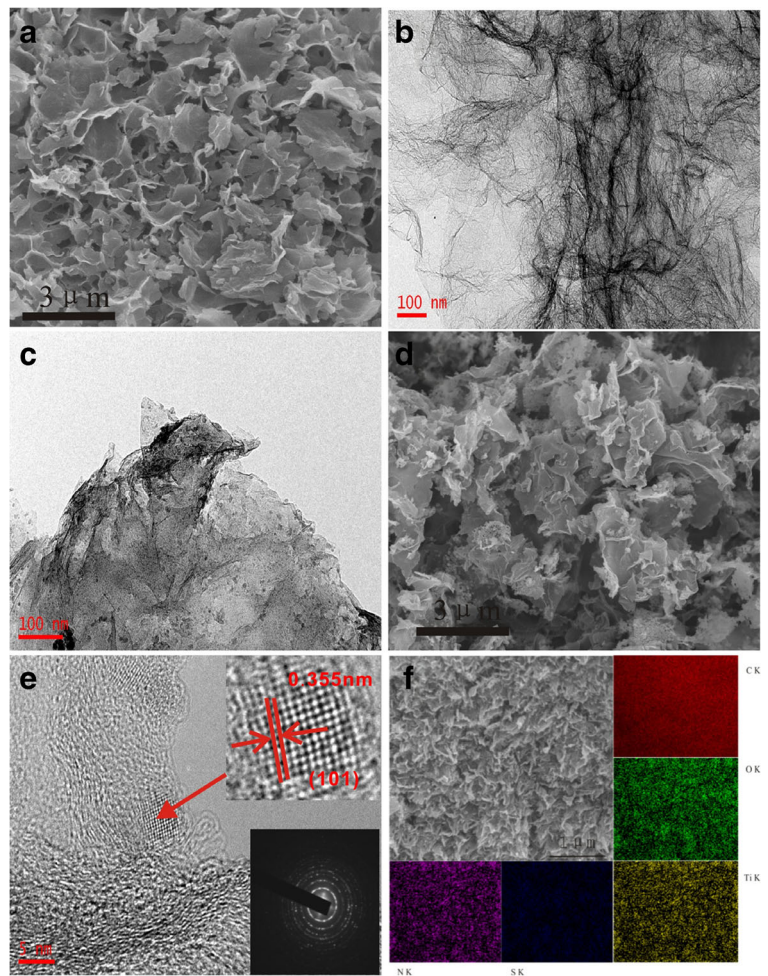
weight loss was about 4%. And when it rose to 400 °C, the carbon in the sample began to combust in the air. The carbon content is calculated to be 15.1%.

Raman spectroscopy analysis was performed to detect the defects and imperfections of the as-prepared samples (Fig. 2b). Two distinctive peaks can be observed at 1350 and 1580 cm⁻¹, corresponding to the D and G band, respectively. The G band is related to sp² bonded ordered graphitic carbon, whereas the D band roots in the defects and the degree of the disorder in the grapheme and carbon-based materials. The relative intensity ratio of the ID/IG is generally estimated to evaluate the level of the graphitic structure disordering. The ID/IG of NSC (1.16) is higher than that of GO (0.857), demonstrating the presence of more structure defects which result from the doping of N and S into graphene sheet. Compared with NSC, the ID/IG ratio of NSC@TiO₂ (1.28) is slightly higher, indicating that the TiO₂ nanoparticles have been infiltrated and the calcination increases the size of the sp² domains.

The XPS was employed to characterize the chemical states of elements in the NSC@TiO₂. The survey spectrum is shown in Fig. 2c, manifests the presence of C, O, N, S, and Ti elements in the sample. The relatively inconspicuous peaks of N and S are ascribed to the low contents in NSC@TiO₂. The N1s peak can be resolved into three peaks centered at 396.85 eV, 398.71 eV, and 401.67 eV (Fig. 2d), corresponding to Pyridinic N, Pyrrolic N, and Graphite N, respectively (Dong et al. 2013; Liu et al. 2013). The S2p spectra can be disintegrated into four peaks at 162.62 eV (sulfide), 167.80 eV (S-S/S-C bonds), 167.90 eV (S-O species), and 168.88 eV (sulfate species) (Fig. 2e) (Dong et al. 2013; Liang et al. 2012; Zhou et al. 2015). Figure 2f shows the spectrum of Ti2p, two peaks at 457.88 and 463.56 eV are assigned to Ti 2p_{3/2} and Ti 2p_{1/2}, respectively (Wang et al. 2015a, b), confirming the formation of TiO₂ in the sample.

N₂ absorption/desorption technique was employed to investigate the porosity of the NSC and NSC@TiO₂, as shown in Fig. 3a, c, the nitrogen sorption isotherms of the as-prepared NSC and NSC@TiO₂ both show type IV isotherm in BDDT (Brunauer, Deming, Deming, and Teller) classification, indicating that the NSC and NSC@TiO₂ have the mesoporous structure. In addition, the hysteresis loop between the adsorption and desorption branches can be assigned as type H3 in the IUPAC

Fig. 1 a, b SEM and TEM images of NSC. c, d SEM and TEM images of NSC@TiO₂. e HRTEM images of NSC@TiO₂. Inset to e is the SAED pattern of NSC@TiO₂ f the SEM elemental mapping images of NSC@TiO₂

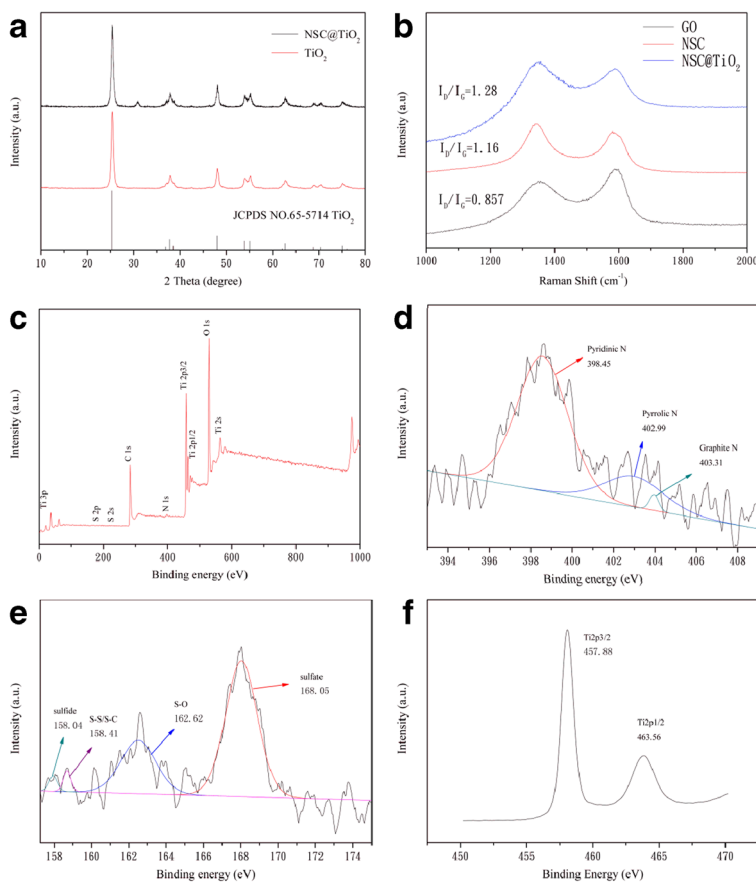


(International Union of Pure and Applied Chemistry) classification, suggesting that the slit-shaped pores are formed. The BET surface area and the pore size calculated based on the BJH desorption curve of NSC were $225 \text{ m}^2 \text{ g}^{-1}$ and $0.25 \text{ cm}^3 \text{ g}^{-1}$, respectively. After the anchoring of TiO₂ nanoparticles, the specific surface area of NSC@TiO₂ decreased to $52.95 \text{ m}^2 \text{ g}^{-1}$ with a total pore volume of $0.17 \text{ cm}^3 \text{ g}^{-1}$, demonstrating the occupation of TiO₂ quantum dots in the pore of the NSC.

CV was employed to investigate the electrochemical performance of the NSC@TiO₂ and TiO₂ at a scan rate of 0.2 mV s^{-1} within a voltage range of 0.01–3 V vs. Li⁺/Li. A couple of cathodic/anodic peaks around 2.1/1.7 V can be observed in Fig. 4a, which were contributed to the lithium ion intercalation and deintercalation of the anatase TiO₂ (Wang and Lou 2012). Figure 3 shows the CV curves of

TiO₂. The peak around 0.6 V can be ascribed to the formation of SEI films. Disappearance of this peak in the subsequent scans suggests the existence of a stable SEI films. As can be seen, the cathodic/anodic peaks of TiO₂ are continually changing, which corresponds to the pore cycle performance of TiO₂. As Fig. 4b shows, the 1st, 2nd, and 200th charge/discharge curves of the NSC@TiO₂ at a current density of 0.2 A g^{-1} do have the plateaus around 1.7/2.1 V, corresponding to the insertion/extraction of lithium to anatase TiO₂, which was in good accordance with the CV curves. After 200 cycles, the plateaus still can be seen, representing a well partial reversibility of the reaction. The initial discharge and charge capacity are about 681 and 412 mAh g^{-1} , demonstrating a coulombic efficiency (CE) of 60.4%. The low CE is mainly caused by the irreversible capacity loss and the formation of SEI films. The NSC@TiO₂ electrode

Fig. 2 **a** XRD pattern of NSC@TiO₂ and TiO₂. **b** Raman spectrum of GO, NSC, and NSC@TiO₂. **c** XPS spectrum of the NSC@TiO₂. **d–f** the corresponding high-resolution N 1s, S 2p, and Ti 2p



exhibits discharge capacity of 439 mAh g⁻¹ after 200 cycles, indicating the outstanding cycling performance of NSC@TiO₂ electrode. The poor reversible capacity of the pure anatase TiO₂ is because of the kinetic problems and the low lithium embedding content.

Figure 4c shows the cycling behavior of NSC, NSC@TiO₂, and the anatase TiO₂ electrodes under a current density of 200 mA g⁻¹. For comparison, the performance of the NSC electrode and the pure anatase TiO₂ electrode were tested in the same electrochemical condition, the NSC electrode and the anatase TiO₂ electrode show a CE of 68.8%, and 65% in the first cycle, respectively. The anatase TiO₂ electrode have the lowest capacity (350.6 mAh g⁻¹ in the first cycle) among the three electrodes and behave badly (116 mAh g⁻¹ after 200 cycles) in the long cycle test because of the poor electrical conductivity and the low Li⁺ diffusion coefficient. The capacity of the first cycle of NSC is 1045.9 mAh g⁻¹, and decreases to 159 mAh g⁻¹ after 200 cycles. The NSC@TiO₂

composite electrode delivered a discharge capacity of 681 mAh g⁻¹ at the first cycle, nevertheless the capacity decreased in the following cycles. This is a common phenomenon for graphene-based material ascribing to the inevitable formation of SEI films and the irreversible reaction of Li⁺ insertion (Ren et al. 2014). After the first 10 cycles, the discharge capacity of NSC@TiO₂ maintained 250 mAh g⁻¹ with a CE of about 99%. And after 450 cycles, the NSC@TiO₂ still remained 248 mAh g⁻¹. The superior cyclic performances are well consistent with the structural stability of TiO₂ and the improved electrical conductivity of doped carbon. The relatively high capacity of the NSC@TiO₂ may come from the synergistic effect of the specific capacity which contributed from the NSC and enhanced surface electrochemistry, heteroatoms doping results in the modification of the structure. Additionally, the mesoporous carbon can promote the electronic conductivity too.

The rate capacities of NSC, NSC@TiO₂, and TiO₂ electrodes were tested at increased current rates of

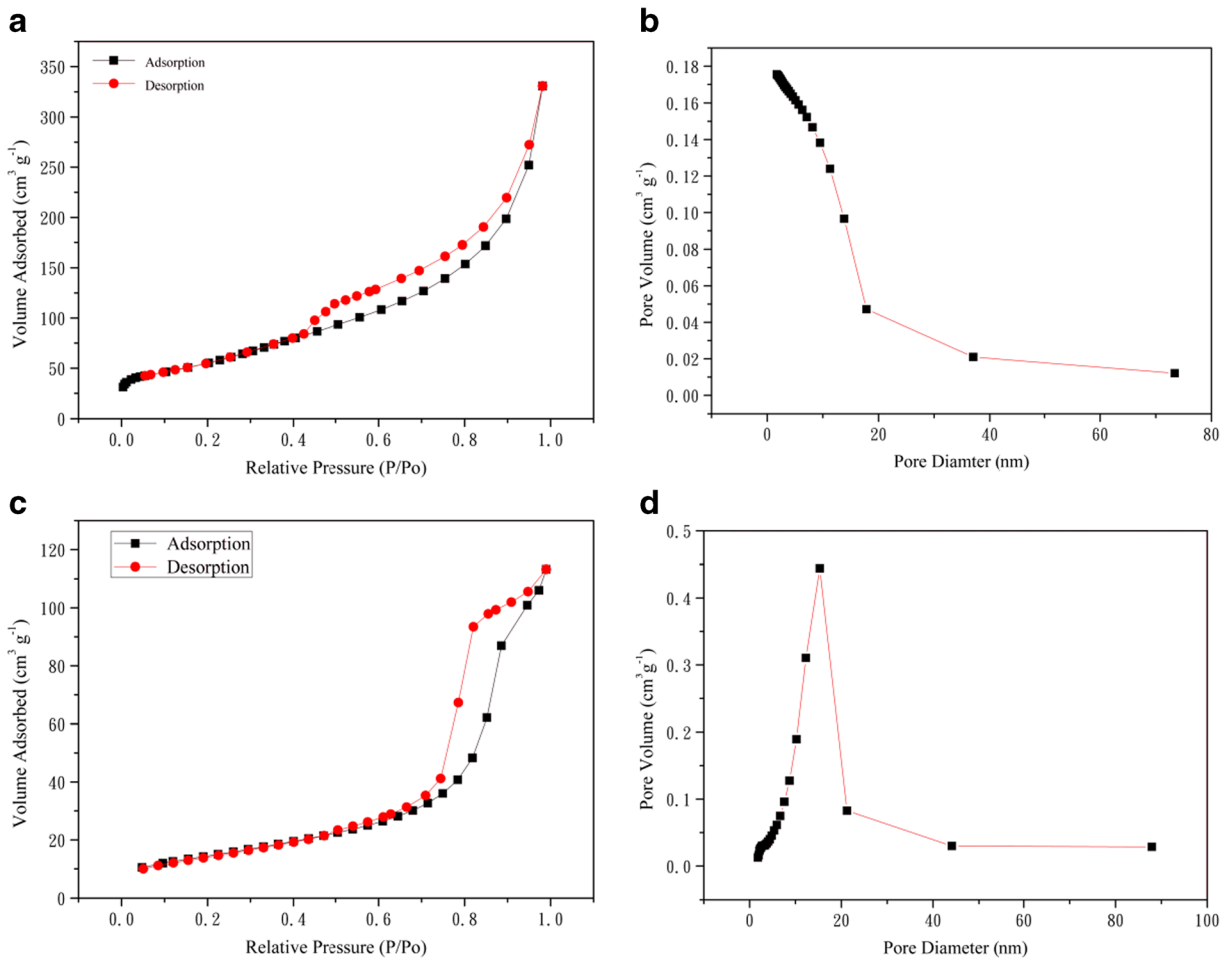


Fig. 3 The nitrogen adsorption-desorption isotherms and corresponding pore size distribution curves of NSC (a, b) and NSC@TiO₂ (c, d)

100, 200, 500, and 1000 mA g⁻¹ to further confirm the improved electrochemical performance. As Fig. 4d shows, the NSC and TiO₂ electrodes reduced rapidly after 10 cycles at the current rate of 100 mA g⁻¹. The capacities of TiO₂ are 248, 186, 132, and 98 mAh g⁻¹ at 0.1, 0.2, 0.5, and 1 Ag⁻¹, respectively, while the NSC electrode delivers 706, 528, 307, and 128 mAh g⁻¹ at each current density. Moreover, the two electrodes cannot resume the capacity when the current density restore back, the TiO₂ electrode remained 124 mAh g⁻¹ and the NSC electrode maintained 386 mAh g⁻¹. The NSC@TiO₂ electrode behaved the best rate capability compared with the other materials as indicated, the NSC@TiO₂ composite electrode exhibits 653, 441, 264, and 140 mAh g⁻¹. Particularly, when the current density returned to 100 mA g⁻¹, the NSC@TiO₂ reverted the reversible capacity of 550 mAh g⁻¹, indicating that the

homogeneous distributed TiO₂ nanoparticles and the highly conductive NSC substrate strengthens the Li⁺ diffusion coefficient, reduce the expansion of volume during the Li⁺ insertion and do necessarily benefit the excellent rate capability.

EIS was employed to investigate the electrochemical kinetics of the electrodes, the Nyquist plots were conducted at the circuit voltage (3 V vs. Li/Li⁺) in the frequency range of 0.01 Hz–100 kHz of the initial discharge. As is shown in Fig. 5, both the anatase TiO₂ electrode and NSC@TiO₂ electrode present a semicircle in the medium to high frequency and a spike in the low frequency region. The semicircle in the moderate frequency region corresponds to the charge transfer resistance, the diameter of the semicircle of the NSC@TiO₂ electrode show a lower value than that of the anatase TiO₂ electrode, demonstrating the lower Li⁺ diffusion resistance.

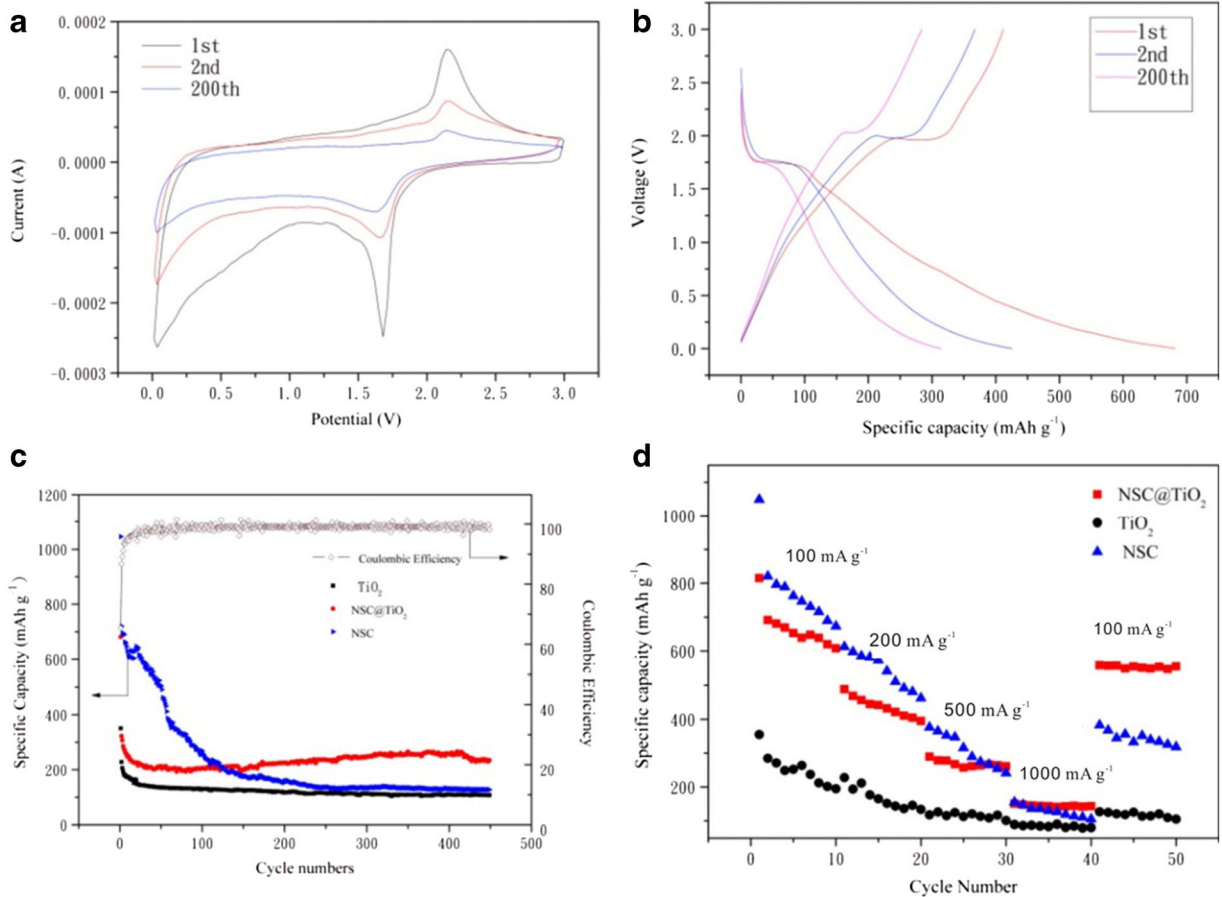


Fig. 4 **a** CV curves of the NSC@TiO₂ at a scan rate of 0.2 mV s⁻¹ for the 1st, 2nd, and 200th cycles. **b** Charge and discharge profiles of NSC@TiO₂ at a current density of 200 mA g⁻¹. **c** Comparative

cycle performance of different samples at a current density of 200 mA g⁻¹. **d** Rate performance of the three samples

Conclusion

In summary, we developed the utilization of N/S dual-doped carbon as framework for the homogeneous

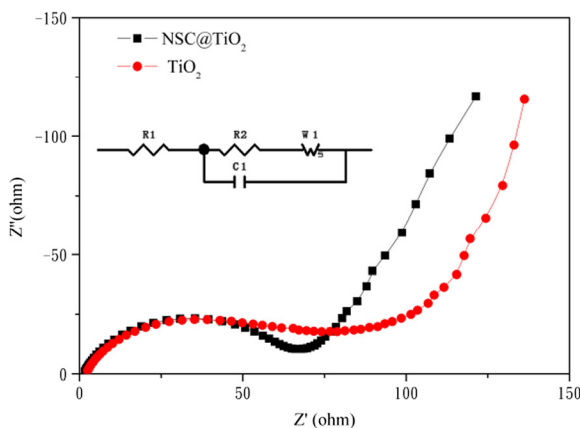


Fig. 5 Nyquist plots of the NSC@TiO₂ and TiO₂

anchoring of TiO₂ nanoparticles. Typically, TiO₂ nanoparticles are anchored into the porous graphene-based sheets with N, S dual doping feature, which is produced by carbonization and KOH activation process. The NSC@TiO₂ electrode presents outstanding behavior with a high initial discharge capacity of 681 mAh g⁻¹ and maintained 220 mAh g⁻¹ after 200 cycles. The excellent cycling performance and superior rate capacity may correspond to the effect of the N/S heteroatoms doping of carbon matrix and the well-defined structure. These results suggest that NSC@TiO₂ is promising to be applied as anode material for LIBs. This work provides an instructive method to enhance the performance of the low-conductive materials in lithium ion batteries.

Funding information This study was funded by the National Nature Science Foundation of China (Grant no. 51204209).

Compliance with ethical standards

Conflict of interest The authors declare that they have no conflict of interest.

References

- Aricò AS, Bruce P, Scrosati B, Tarascon JM, Van SW (2005) Nanostructured materials for advanced energy conversion and storage devices. *Nat Mater* 4(5):366–377
- Armand M, Tarascon JM (2008) Building better batteries. *Nature* 451(7179):652–657
- Beaulieu LY, Larcher D, Dunlap RA, Dahn JR (2000) Reaction of Li with grain-boundary atoms in nanostructured compounds. *J Electrochem Soc* 147(9):3206
- Belharouak I, Sun YK, Lu W, Amine K (2007) On the safety of the Li₄Ti₅O₁₂/LiMn₂O₄ lithium-ion battery system. *J Electrochem Soc* 154(12):A1083–A1087
- Chen Z, Belharouak I, Sun YK, Amine K (2013) Titanium-based anode materials for safe lithium-ion batteries. *Adv Funct Mater* 23(8):959–969
- Chu S, Zhong Y, Cai R, Zhang Z, Wei S, Shao Z (2016) Mesoporous and nanostructured TiO₂ layer with ultra-high loading on nitrogen-doped carbon foams as flexible and free standing electrodes for lithium-ion batteries. *Small* 12(48):6724–6734
- Dong Y, Pang H, Yang HB, Guo C, Shao J, Chi Y, Li CM, Yu T (2013) Carbon-based dots co-doped with nitrogen and sulfur for high quantum yield and excitation-independent emission. *Angew Chem* 125(30):7954–7958
- Hummers WS Jr, Offeman RE (1958) Preparation of graphitic oxide. *J Am Chem Soc* 80(6):1339
- Jannik J, Maier J (2004) Nanocrystallinity effects in lithium battery materials. *Aspects of nano-ionics. Part 4. Cheminform* 35(4):5215–5220
- Jung HG, Jang MW, Hassoun J, Sun YK, Scrosati B (2011) A high-rate long-life Li₄Ti₅O₁₂/Li_{0.45}Co_{0.1}Mn_{1.45}O₄ lithium-ion battery. *Nat Commun* 2(7):516
- Kamata M, Fujine S, Yoneda K, Kanda K, Esaka T (1999) Diffusion coefficient measurement of lithium ion in sintered Li_{1.33}Ti_{1.67}O₄ by means of neutron radiography. *Solid State Ionics* 123(1):165
- Larcher D, Tarascon JM (2015) Towards greener and more sustainable batteries for electrical energy storage. *Nat Chem* 7(1):19–29
- Liang J, Jiao Y, Jaroniec M, Qiao SZ (2012) Sulfur and nitrogen dual-doped mesoporous graphene electrocatalyst for oxygen reduction with synergistically enhanced performance. *Angew Chem Int Ed Engl* 51(46):11496
- Liu Z, Nie H, Yang Z, Zhang J, Jin Z, Lu Y, Xiao Z, Huang S (2013) Sulfur-nitrogen co-doped three-dimensional carbon foams with hierarchical pore structures as efficient metal-free electrocatalysts for oxygen reduction reactions. *Nanoscale* 5(8):3283–3288
- Ma X, Ning G, Sun Y, Pu Y, Gao J (2014) High capacity Li storage in sulfur and nitrogen dual-doped graphene networks. *Carbon* 79(6):310–320
- Mi JEC, Nam KM, Lee Y, Song K, Park JT, Kang YM (2011) Phosphidation of Li₂O nanoparticles and their electrochemical and biocompatible superiority for lithium rechargeable batteries. *Chem Commun* 47(41):11474–11476
- Qiu B, Xing M, Zhang J (2014) Mesoporous TiO₂ nanocrystals grown in situ on graphene aerogels for high photocatalysis and lithium-ion batteries. *J Am Chem Soc* 136(16):5852–5855
- Ren H, Yu R, Wang J, Jin Q, Yang M, Mao D, Kisailus D, Zhao H, Wang D (2014) Multishelled TiO₂ hollow microspheres as anodes with superior reversible capacity for lithium ion batteries. *Nano Lett* 14(11):6679–6684
- Shen L, Yuan C, Luo H, Zhang X, Chen L, Li H (2011) Novel template-free solvothermal synthesis of mesoporous Li₄Ti₅O₁₂-c microspheres for high power lithium ion batteries. *J Mater Chem* 21(38):14414–14416
- Tarascon JM, Armand M (2001) Issues and challenges facing rechargeable lithium batteries. *Nature* 414:359–367
- Wagemaker M, van Eck ERH, Kentgens APM, Mulder FM (2009) Li-ion diffusion in the equilibrium nanomorphology of spinel Li_{4+x}Ti₅O₁₂. *J Phys Chem B* 113:224–230
- Wang Z, Lou XW (2012) TiO₂ nanocages: fast synthesis, interior functionalization and improved lithium storage properties. *Adv Mater* 24(30):4124–4129
- Wang X, Sun G, Routh P, Kim DH, Huang W, Chen P (2014a) Heteroatom-doped graphene materials: syntheses, properties and applications. *Chem Soc Rev* 43(20):7067–7098
- Wang X, Weng Q, Liu X, Wang X, Tang DM, Tian W, Zhang C, Yi W, Liu D, Bando Y, Golberg D (2014b) Atomistic origins of high rate capability and capacity of n-doped graphene for lithium storage. *Nano Lett* 14(3):1164–1171
- Wang H, Ma C, Yang X, Han T, Tao Z, Song Y, Liu Z, Guo Q, Liu L (2015a) Fabrication of boron-doped carbon fibers by the decomposition of b₄c and its excellent rate performance as an anode material for lithium-ion batteries. *Solid State Sci* 41:36–42
- Wang C, Wu L, Wang H, Zuo W, Li Y, Liu J (2015b) Fabrication and shell optimization of synergistic TiO₂-MoO₃ core-shell nanowire array anode for high energy and power density lithium-ion batteries. *Adv Funct Mater* 25(23):3524–3533
- Wu L, Yang J, Zhou X, Tang J, Ren Y, Yang N (2016) Enhanced electrochemical performance of heterogeneous Si/MoS₂ anodes prepared by a magnesiothermic reduction. *ACS Appl Mater Interfaces* 8(26):16862
- Xing LB, Hou SF, Zhang JL, Zhou J, Li Z, Si W, Zhuo S (2015) A facile preparation of three dimensional n, s co-doped graphene hydrogels with thiocarbonylhydrazide for electrode materials in supercapacitor. *Mater Lett* 147:97–100
- Yang J, Xi L, Tang J, Chen F, Wu L, Zhou X (2016) Three-dimensional porous carbon network encapsulated SnO₂ quantum dots as anode materials for high-rate lithium ion batteries. *Electrochim Acta* 217:274–282
- Yu Z, Song J, Gordin ML, Yi R, Tang D, Wang D (2015) Phosphorus-graphene nanosheet hybrids as lithium-ion anode with exceptional high-temperature cycling stability. *Adv Sci* 2(1–2). <https://doi.org/10.1002/adv.201400020>
- Yun YS, Le VD, Kim H, Chang SJ, Baek SJ, Park S et al (2014) Effects of sulfur doping on graphene-based nanosheets for

- use as anode materials in lithium-ion batteries. *J Power Sources* 262(4):79–85
- Zhao L, Hu YS, Li H, Wang Z, Chen L (2011) Porous $\text{Li}_4\text{Ti}_5\text{O}_{12}$ coated with n-doped carbon from ionic liquids for Li-ion batteries. *Adv Mater* 23(11):1385–1388
- Zhou G, Paek E, Hwang GS, Manthiram A (2015) Long-life Li/polysulphide batteries with high sulphur loading enabled by lightweight three-dimensional nitrogen/sulphur-codoped graphene sponge. *Nat Commun* 6:7760
- Zhou X, Xi L, Chen F, Bai T, Wang B, Yang J (2016) In situ growth of SnO_2 nanoparticles in heteroatoms doped cross-linked carbon frameworks for lithium ion batteries anodes. *Electrochim Acta* 213:633–640
- Zhuang GL, Bai J, Tao X, Luo JM, Wang X, Gao Y, Zhong X, Li XN, Wang JG (2015) Synergistic effect of s,n-co-doped mesoporous carbon materials with high performance for oxygen-reduction reaction and Li-ion batteries. *J Mater Chem A* 3(40):20244–20253